Chapter 7

OPTIMAL MANEUVERING TRAJECTORY FOR FINS OF LARGE ASPECT RATIO

Nature's swimmers have evolved to adapt to their surrounding environment and mode of life. Chapter 6 has detailed the difference between large cruisers, who have developed a lift-based locomotive mechanism that results in high propulsive efficiency, and fish that dwell in reefs, who have evolved to use drag-based or combined propulsion methods that result in lower propulsive forces but higher maneuverability in the conditions they encounter. It should be clarified that these drag-based mechanisms result in higher maneuverability at low swimming velocities only. As swimming speed is increased the fin and flow velocity approach each other, and the force generated by the fin is largely reduced (Fish, 2013; Vogel, 1994). Fast swimmers typically employ lift forces to maneuver, resulting, however, in larger turning radii (Fish, 2002; Maddock et al., 1994).

Associated to these environmental and propulsive variations is a difference in body and fin morphology (Webb, 1984). Fish with different modes of life possess different sets of fins, with their shape varying according to their functionality. Low-aspect-ratio oar-type fins are more suited for drag-based paddling (Blake, 1981), while high aspect ratio fins generate lift forces more efficiently (Walker and Westneat, 2002). This improved efficiency is analogous to the reduction of drag in high-aspect-ratio wings and is a consequence of the reduction in the induced drag caused by the tip vortices. For this reason, thunniform swimmers typically possess high-aspect-ratio, lunate-shaped caudal fins (Lighthill, 1969; Sambilay Jr et al., 1990).

To achieve both high maneuverability at low velocities and high efficiency Martin and Gharib (2018) employed the current experimental setup to explore the trajectory to be followed by a fin of AR=1, which lies between those of cruisers and maneuvering specialists and was considered a good compromise for a generalist design. They performed two tests that searched for the most efficient trajectory to generate a side force of F=17mN. The first test corresponded to a fully three-dimensional trajectory. In the second test, the degrees of freedom were limited such that the trajectory of the fin's centerpoint was a straight line. The parameters of the optimal trajectories that resulted are shown in table 7.1. The 2D projection of the trajectories is shown together with the resulting forces in figures 7.1 (fully 3D trajectory) and 7.2 (trajectory limited to a line). For each interval illustrated in these figures, the motion of the fin starts at the point indicated with a diamond. To facilitate comparison, the trajectories have been rotated such that the average force is aligned with the x' direction. It must be noted that these figures have been extracted from Martin and Gharib (2018) and the notation and orientation is not fully consistent with the one employed in throughout the remaining of this text.

The trajectory that resulted from the fully three-dimensional optimization follows a paddling strategy. In the upstroke (figure 7.1a) the fin is oriented as perpendicular as possible to the x' direction, while its motion aligns as much as possible with that direction, generating a large drag force that is aligned with x'. In the downstroke (figure 7.1b) the fin aligns with the x' direction, minimizing the forces generated. The trajectory that resulted from the limited optimization is shown in figure 7.2 and seems to follow a lift-generating strategy. The fin is oriented at an angle to the direction of its motion, and the $F_{x'}$ force is positive during 82% of the cycle. It is interesting to note that the efficiency of the trajectory that is limited to a line ($\eta = 0.413$) is higher than the efficiency of the fully three-dimensional trajectory ($\eta = 364$), despite it being a subset of the latter. This highlights one of the limitations of this procedure: there is no guarantee that the optimum obtained will be a global optimum. It will represent, nonetheless, a good general strategy that achieves the desired force and constitutes an optimal configuration if considering small variations around it.

The results of Martin and Gharib (2018) demonstrate the feasibility of an AUV design that retains a rigid body and utilizes a caudal fin for both propulsion and maneuvering. The low aspect ratio of the fin selected as a compromise in their study will result, however, in reduced propulsive efficiency with respect to that achievable by higher aspect ratios. The importance of the degrees of freedom of a fish fin in its performance has been emphasized in the literature (Lauder and Drucker, 2004). While it is unlikely that the three-degree-of-freedom mechanism employed here will significantly improve the propulsive efficiency with respect to fish locomotion, it is probable that it could result in improved maneuverability. The approach of the current study is, therefore, to retain nature's thunniform design, and in particular the high aspect ratio of the fin, for high cruising efficiency and explore the ability of the mechanism to produce turning forces by performing motions that are, perhaps, not available to fish due to more restrictive physical constraints. In this chapter,

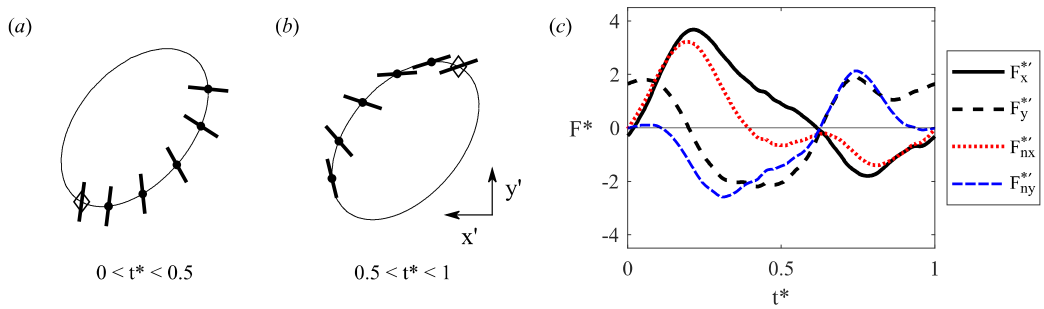

Figure 7.1: The forward stroke (a) and the backwards stroke (b) of the rotated optimal trajectory for generating side-force. The diamond corresponds to the position of the fin at the start of each stroke. The corresponding $F*_x{}'$, $F*_y{}'$, $F*_{n_x}{}'$ and $F*_{n_x}{}'$ (c) show the instantaneous phase averaged forces over a single cycle as a function of $t*$. Extracted from Martin and Gharib (2018) DOI:10.1088/1748-3190/aaefa5

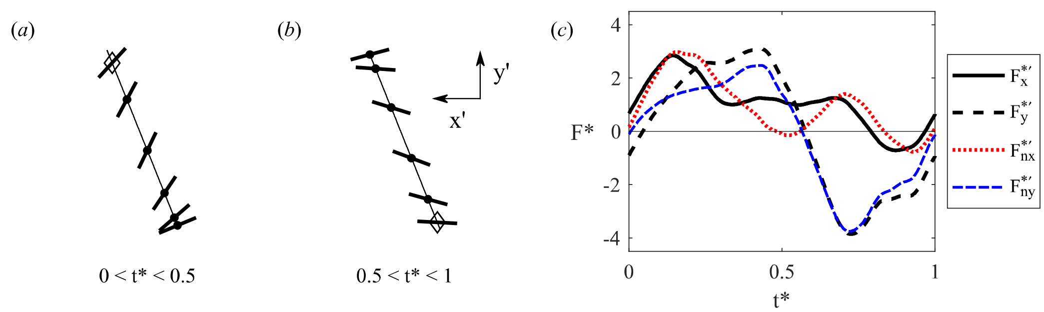

Figure 7.2: The upward stroke (a) and the downward stroke (b) of the rotated optimal trajectory for generating side-force when the trajectory is limited to a line. The diamond corresponds to the position of the fin at the start of each stroke. The corresponding $F*_x{}'$, $F*_y{}'$, $F*_{n_x}{}'$ and $F*_{n_x}{}'$ (c) show the instantaneous phase averaged forces over a single cycle as a function of $t*$.Extracted from Martin and Gharib (2018) DOI:10.1088/1748-3190/aaefa5

the optimal trajectory for a fin of aspect ratio AR=4, which is in the lower limit for the caudal fin of thunniform swimmers, will be analyzed, with the ambition of converging on a design that is not only agile but also possesses propulsive efficiencies close to those of nature.

7.1 Results

Optimal trajectory for a fin of AR=4

The optimal trajectory, as defined by equation 6.1, followed by a fin of AR=4 to generate a side force of $F_{target} = 17$mN was searched using the optimization procedure described in chapter 6. The resulting parameters are presented in table 7.1. The two-dimensional projection of the corresponding trajectory is illustrated in figure 7.3. It is divided into four segments to avoid cluttering; their temporal order is counterclockwise (I-IV). These do not correspond to equal time intervals but have rather been divided according to separate characteristic maneuvers. For simplicity of comparison, the trajectories have been rotated such that the resulting force is in the x' direction. This resulting force is plotted in figure 7.3b, together with the modulus of the forces normal and tangential to the fin (in the x and y axis represented in figure 6.3b, respectively). The forces have been non-dimensionalized with the target force $\tilde{F} = F/F_{target}$, such that the integral of $\tilde{F_{x'}}$ over a cycle is approximately equal to one, and the time has been non-dimensionalized with the period of the motion $\tilde{t} = tf$. Figure 7.3c displays the normal velocities of the two edges of the fin (blue and red, corresponding to blue and red points in figure 7.3a) and the centerpoint (black), non-dimensionalized with the average tip velocity U_{tip} over the period. The intervals corresponding to each segment I-IV of the trajectory are marked by vertical lines in this plot, as well as figure 7.3b. Unlike the trajectories obtained by Martin and Gharib (2018) for a fin of AR=1, that corresponded to paddling and lift-based mechanisms, the strategy and force generating mechanisms of the trajectory are no longer evident. As will be clarified below, several different mechanisms are combined within the single trajectory to generate the optimal strategy.

The first consideration that should be made in order to interpret the resulting trajectory is related to the wing's geometry. Wings of low aspect ratio will generate large forces when rotated around their x and y axis, as shown in figure 6.3b. This is a result of the fin and arm lengths being large compared to the other dimensions, producing substantial velocities at the wing tip that will generate large forces. Rotations around the z axis, on the other hand, will result in smaller velocities and forces. In the case of a fin of large aspect ratio, however, the width of the fin is also large, and rotations around its z axis will generate significant velocities at the edges, resulting in considerable forces. A substantial portion of the forces produced by the fin of AR=4 are generated by rotation around its z-axis. A fin that rotates around its centerpoint, however, will generate no net force. In the optimal trajectory, the motion of the centerpoint and the rotation around the fin's z axis are combined

Parameter	Symbol	AR=1 3D	AR=1 Line	AR=4 3D	AR=4 Line
Type	—	Ellipse	—	Ellipse	—
Stroke angle	ϕ	27.9°	28.3°	36.0°	36°
Deviation angle	ψ	15.7°	0°	19.9°	0°
Rotation angle	χ	63°	44.1°	−70°	−48.5°
Rotation phase	β	4.4	3.2	0	6.1
Rotation acceleration	K_v	0.2	0.1	0.2	0.5
Speed-up code	S	0	2	2	1
Speed-up value	γ	1	1.2	1	1.2
Camber	λ	0.1	0	0.4	0
Frequency	f	0.19 Hz	0.19 Hz	0.19 Hz	0.2Hz
Force	$F_{x'}$	16.95mN	16.97mN	17.07mN	16.89mN
Efficiency	η	0.364	0.413	0.829	0.555

Table 7.1: Parameters of optimal trajectories for rigid fins. Data for the fins of AR=1 has been extracted from Martin and Gharib (2018).

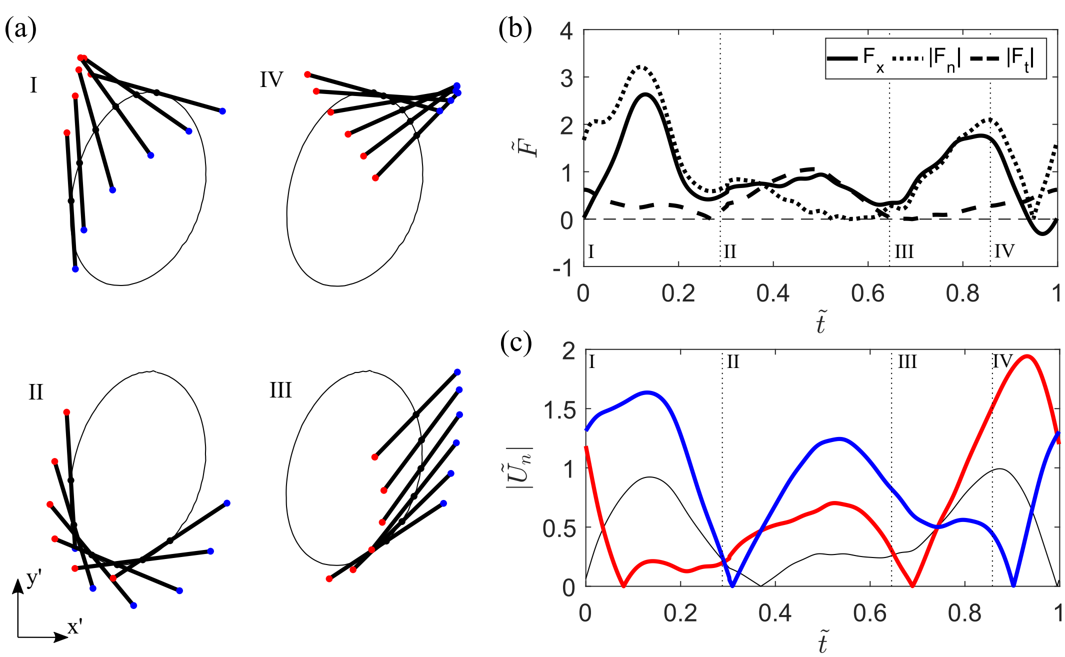

Figure 7.3: (a) Optimal trajectory for a rigid fin of AR=4, where the sequence is I-IV. (b) Resulting side force, $F_{x'}$, normal force and tangential force. (c) Normal velocity of fin edges and centerpoint, with the colors corresponding to the points in (a)

to modify the overall center of rotation, that moves towards one of the fin's edges. This is evident in segments I and IV of the trajectory, illustrated in figure 7.3. It is emphasized in figure 7.3c. During segment I of the trajectory, the velocity of the red edge decreases to zero and plateaus at a low value, while the velocity of the blue edge reaches its maximum. The fin rotates around the red edge, generating forces that are oriented in the desired direction. In segment IV of the trajectory, on the other hand, the fin rotates around the blue edge, generating forces that are still in the desired direction. This two-step rotation allows the fin to undergo large rotations around its z axis while always producing favorable forces. Segment III of the trajectory represents the opposite case; the rotation around the fin's z axis has been combined with the curvature of the centerpoint's trajectory such that practically no normal force is generated by the rotation. The motion of the fin throughout the different segments as well as the resulting fluid forces are described in detail in the following paragraphs.

The mechanism responsible for the generation of momentum during the rotation in segment I can be inferred from the geometry of the trajectory and the fin's velocity, shown in figures 7.3a and b, respectively. Because the angle swept is large and the fin is oriented perpendicularly to its motion, the possible responsible forces are either form drag or acceleration reaction. The velocity of the blue and red edges is practically constant throughout a significant part of segment I, which is inconsistent with an acceleration reaction being responsible for the large normal force. Additionally, the velocity of the blue edge decreases rapidly in the second half, which results in an added mass force in the negative x' direction. The large positive peak in $F_{x'}$ is therefore caused by a form drag force. This is further supported by the observation that the peak force and maximum velocity coincide in time. As the fin aligns its normal with the x' direction, a larger proportion of the normal force is in the desired direction, resulting in $F_{x'}$ and $|F_n|$ overlapping at the end of this rotation.

Throughout segment II of the trajectory, the fin performs a rotation such that it is positioned practically tangent to the trajectory of its centerpoint at all times, resulting in a normal force that approaches zero (figure 7.3b). The tangential force, on the other hand, sees a significant increase in this segment and is responsible for most of the force in the x' direction. Because the normal force is present in the denominator of the efficiency (equation 6.1), the presence of a force in the x' direction when the normal force is small significantly increases the value of the efficiency. Surprisingly, the tangential force is not caused by the friction drag generated by the motion of the plate, which produces a force in the negative x' direction (figure 7.3). The mechanism creating this positive tangential force is not evident, but may be related to the fin's inertia, the non-stagnant flow the fin encounters as a result of the previous stroke and unsteady mechanisms involving the vortex dynamics, which are rich in this motion. A visualization of the flow structures can be viewed in figure 7.4.

Segment III of the trajectory corresponds to a power stroke, with the main contributor to the force in the x' direction being the normal force. The motion of the fin is practically perpendicular to the force generated, which indicates that it corresponds to a lift mechanism. The value of the force follows a similar trend to that of the velocity of the fin's centerpoint, which is an indicator of a velocity-dependent force such as lift. Flow visualization (figure 7.4) reveals a vortex forming at the fin's leading edge (blue edge), which is shed towards the end of the segment.

The beginning of segment IV is characterized by a decrease in the normal force experienced by the fin, caused by the competing action of a drag force and an acceleration reaction force. The clockwise rotation of the fin generates a drag force that has a component in the positive x' and negative y' direction. Figure 7.3c, shows, however, a deceleration in the motion of the centerpoint, combined with a decrease in velocity of the blue edge that is followed by an acceleration in the opposite direction and a small increase in the velocity of the red edge followed by a deceleration. This overall deceleration results in an added mass that will generate an opposing acceleration reaction force, in the negative x' and positive y' direction, over most of the fin. As the fin crosses the horizontal position, the sign of the x' component of the normal is reversed, resulting in a negative contribution to the $F_{x'}$ force. The subsequent acceleration of the wing in the opposite rotation direction (deceleration of the red edge and acceleration of the blue edge) at the end of segment IV causes the $F_{x'}$ force to return to the positive values. The added mass force is dominant up to the time at which the velocity stagnates, which corresponds to the initial stage of segment I. An inflection point can be observed in the curve of the normal force at this point. The full cycle is then repeated to generate an overall force in the $F_{x'}$ direction.

These observations provide an outline of the general characteristics of the fin's motion and the forces produced. They do not, however, account for more complex unsteady fluid phenomena such as the shedding of vorticity and dynamics of the vortices. Unsteady flow phenomena such as delayed stall and wake capture are fundamental to the performance of insect flight (Dickinson et al., 1999), and are

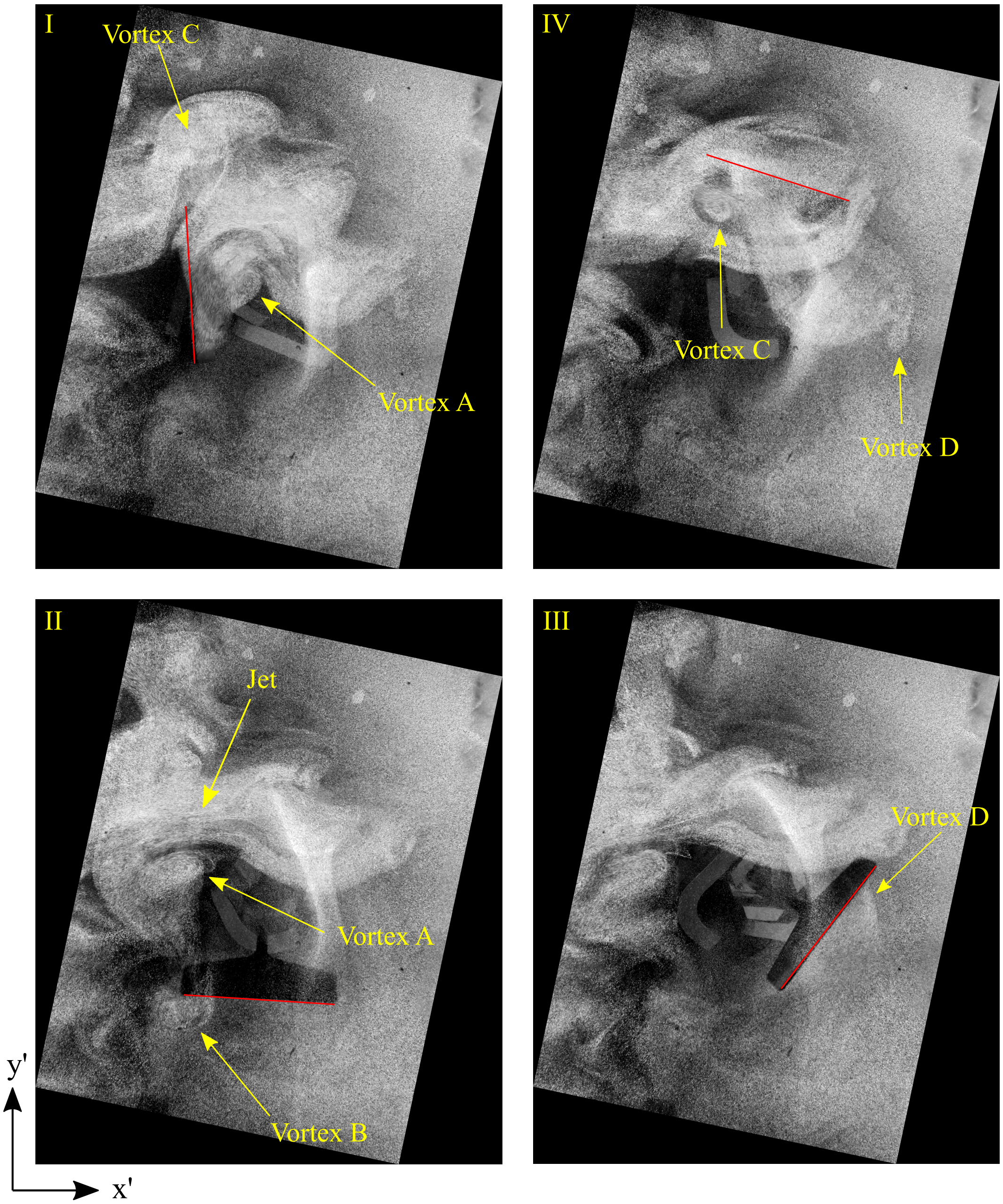

Figure 7.4: Flow visualization of the optimal trajectory obtained for a rigid fin of AR=4. The edge of the fin is highlighted in red.

likely to play an important role in this complex three dimensional fin motion. Although these vortices are not the major providers of force, their presence does alter the forces exerted on the fin and may be responsible for the optimality of the trajectory over other similar trajectories. Due to the complexity of the trajectory, a comprehensive and quantitative analysis of these effects would require three-dimensional velocimetry, which is beyond the scope of this work. Qualitative flow visualization has been performed, however, to highlight the general features of the flow. Four images are presented in figure 7.4, each corresponding to the plate in one of the four segments of its motion. In a similar manner to figure 7.3a, the temporal evolution in this figure is counterclockwise.

A leading edge vortex (vortex A, figure 7.4 I) is formed during the large rotation of segment I, where the leading edge corresponds to the blue edge in figure 7.3a. This vortex detaches close to the end of the rotation and rolls over the fin's upper surface. It is shed over the opposite red edge of the fin at the beginning of segment II. A high-velocity jet is generated in the negative x' direction (figure 7.4 II). Its velocity is imparted by the fin's motion both in segment I and segment III of the trajectory. After its detachment, vortex A moves in the negative x' direction together with this jet. A second vortex is formed in the proximity of the leading edge (blue edge) at the beginning of segment II (vortex B, figure 7.4 II). It moves along the bottom surface of the fin and is shed at the red trailing edge, continuing in a downwards (negative y') motion. A third vortex (vortex D, figure 7.4 III) starts forming at the fin's leading edge at the beginning of segment III and is shed at towards the end of the segment. The shed vortex tube can be observed in figure 7.4 IV. It is interesting to note that the motion of the fin in segment III induces a flow with velocity in the positive y' direction, which is encountered by the fin in its downward motion in segment I and enhances the drag force produced. An additional leading edge vortex (vortex C, figure 7.4 IV) is generated at the bottom surface leading edge (red edge) of the fin during the rotation in segment IV. A second vortex, not pictured here, is formed at the top surface at the end of this rotation. Both of these vortices are shed at the red edge as the fin's displacement direction shifts and move upwards (in the positive y' direction) as a vortex pair. Although a simplified description has been provided, as is visible in these images the vortex dynamics of the motion are quite complex, with components in all three dimensions and vorticity being generated in the top and bottom edges of the fin in addition to the blue and red leading edges.

Effect of three-dimensionality and large rotation

The benefits of employing a mechanism that allows for large rotations and three-dimensional motion to generate maneuvering forces with a high aspect ratio fin is now analyzed. The trajectory parameters that are characteristic of this type of motion are the deviation angle, ψ, and the rotation angle, χ, as described in figure 6.2b. Due to physical constraints, the values of both of these variables are very limited in the motions achievable by the caudal finds of thunniform swimmers. The values of these parameters for the optimal trajectory can be found in table 7.1, while the limits on these variables set for this optimization can be viewed in table 6.1. Notably, both the deviation angle and the rotation angle of the optimal trajectory are both at their maximum absolute values (ψ=20°, $\chi = -70°$), which highlights the importance of the parameters in performing efficient maneuvering motions and explains the absence of such a trajectory in nature.

In order to further consider the effect of the trajectory's three-dimensionality, the optimization algorithm was employed to obtain the optimal trajectory that generates a side force of $F_{x'} = 17mN$ considering only the family of trajectories whose centerpoint motion is limited to a straight line. This is performed by setting the values of the deviation angle and camber to zero. The parameters of the resulting optimal trajectory are shown in table 7.1. The average force obtained approaches reasonably well the target force. The efficiency of the trajectory is, however, significantly lower than that of the fully three-dimensional case, being comparable to that obtained by Martin and Gharib (2018) for a fin of AR=1.

The trajectory's two-dimensional projection is shown in figure 7.5a, where the starting point of the fin at each of the two segments is marked with a square. The corresponding forces and velocities have been plotted in figures 7.5b and c, respectively, in a similar manner to figure 7.3. The trajectory has been rotated such that the average force is in the x' direction. In a similar manner to a paddling motion, the trajectory followed by the fin is divided into a power stroke (segment I) and a recovery stroke (segment II). The majority of the favorable force is generated during the power stoke, while the recovery stroke is limited to reducing the forces generated.

Using a similar argument to that of the three-dimensional trajectory, the principal mechanism responsible for the large normal force in the power stroke can be determined to be drag: while the plate is decelerating in the second half of the stroke, the force is still in the positive x' direction. It follows closely, additionally, the curve of

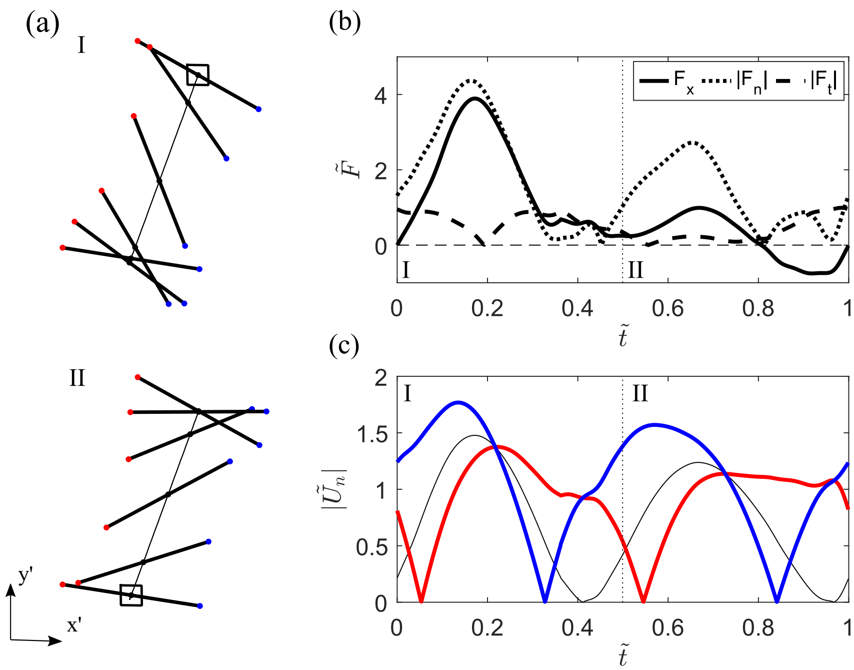

Figure 7.5: (a) Optimal trajectory for a rigid fin of AR=4 when its centerpoint motion is constrained to a line, where the initial position is marked by a square (b) Resulting side force, $F_{x'}$, normal force and tangential force. (c) Normal velocity of fin edges and centerpoint, with the colors corresponding to the points in (a)

the centerpoint velocity. In this constrained case, there is no possibility of combining the centerpoint motion and fin rotation around its z axis to produce favorable large drag-producing turns; although the velocity of the red edge decreases to zero, which must always be the case, it does not remain at a low value. The forces in this stroke are generated, in their majority, by the rotation around the fin's y axis, as represented in figure 6.3, and the parameters of the trajectory have converged accordingly to maximize the force in this power stroke. The speed up value, $\gamma = 1.2$, is high, with the speed code being S=1, which corresponds to a speed up in the power stroke. This results in a peak force that is higher than that of the three-dimensional case. The rotation acceleration, $K_v = 0.5$, is higher than in the three-dimensional case, which results in the fin's rotation being concentrated at the edges of the trajectory, while only small rotations occur at the center. Notably, significant tangential forces are present during the rotation of the fin at the edges of the trajectory and are responsible for a large proportion of the force in the x' direction in those intervals. The origin of this tangential force is not clearly distinguishable, but may be related to inertial effects and vortex dynamics, which are known to be a significant factor in the rotation at stroke reversal for insect flight (Dickinson et al., 1999). While the forces generated at stroke reversal of the optimal trajectory are favorable at the end of the power stroke, they are detrimental at the end of the recovery stroke. During the recovery stroke, the force in the x' direction is small, with the majority of the normal force being oriented in the y' direction. The normal force in the recovery stroke, in a similar manner to the power stroke, is mostly a result of form drag.

It is interesting to note that the rotation angle of this optimal trajectory, $\chi = -48.5°$, is still high in comparison to the rotations achievable by the caudal fins of thunniform swimmers. It therefore constitutes an improvement with respect to the traditional bio-mimetic maneuvering fin motions. Despite this fact, the efficiency is significantly lower than that of the fully three-dimensional case.

7.2 Conclusions

The optimal trajectory that generates a side force of $F_{x'} = 17mN$ for a fin of aspect ratio AR=4 has been obtained utilizing an experimental optimization procedure. The optimum obtained possesses a high deviation angle (i.e., high three-dimensionality) and high rotation angle, which are achievable by the current mechanism but not by the caudal fin of fish due to mechanical constraints. This trajectory results in a remarkably high efficiency, which is twice as large as the optimal trajectory obtained by Martin and Gharib (2018) for a fin of AR=1.

The optimal trajectory uses the combination of four different maneuvers to generate forces efficiently. In the first segment of the trajectory, the plate combines the motion of its centerpoint with the rotation around its z axis to produce an overall rotation that results in a high favorable drag force. In the second segment, the fin moves practically tangentially to the trajectory of its centerpoint, reducing the normal force but generating a tangential force with a component in the x' direction. In the third segment the fin employs a lift mechanism to generate a second high $F_{x'}$ peak. The final fourth segment corresponds to a rotation, where the fin does not generate significant favorable forces but decelerates to its initial position without producing detrimental effects.

A second optimization, where the trajectory of the centerpoint was limited to a line, was performed and a paddling-type strategy was recovered. The sharp decrease in efficiency highlighted the importance of three-dimensionality in generating an efficient turning maneuver for fins of high aspect ratio. Because the propulsive efficiency of lift-based flapping propellers has been shown to be higher for fins of large aspect ratio, the utilization of a mechanism that allows for these high rotations and high three-dimensionality in the fin's motion, and can therefore generate side forces efficiently for large aspect ratio fins, is a promising candidate for an unmanned underwater vehicle that requires both high propulsive efficiency and high maneuverability.